The influence of excitedstate vibrations on fragment state distributions: The photodissociation of NOCl on T1(13A')

C. X. W. Qian, A. Ogai, L. Iwata, and H. Reisler

Articles you may be interested in

Threedimensional analytical infinite order sudden quantum theory for triatomic photodissociation: Dependence on initial rotational and vibrational state and on thermal averages for NOCl dissociation on T 1(1 3 A') surface
J. Chem. Phys. **100**, 9215 (1994); 10.1063/1.467257

Excitedstate preparation and relaxation in the vibrational quasicontinuum
J. Chem. Phys. **95**, 3232 (1991); 10.1063/1.460880

Photodissociation of ammonia at 193.3 nm: Rovibrational state distribution of the NH2(Ã2 A 1) fragment
J. Chem. Phys. **94**, 4195 (1991); 10.1063/1.460653

Stateselective photodissociation dynamics of NOCl: The influence of excited state bending and stretching vibrations
J. Chem. Phys. **89**, 6547 (1988); 10.1063/1.455374

The distribution of vibrationally excited states in resonant radiation and the rate of photodissociation
J. Appl. Phys. **49**, 852 (1978); 10.1063/1.324615

The influence of excited-state vibrations on fragment state distributions: The photodissociation of NOCl on $T_1(1\,{}^3A'')$

C. X. W. Qian, A. Ogai,[a] L. Iwata,[a] and H. Reisler
Department of Chemistry, University of Southern California, Los Angeles, California 90089-0482

NO V,R distributions are reported following photodissociation of jet-cooled NOCl from selected vibrational levels of the T_1 ($1\,{}^3A''$) state. By varying the photolysis wavelength while monitoring selected rovibrational levels of NO, a photofragment yield spectrum showing the same diffuse vibrational structure as the absorption spectrum is obtained. NO rotational distributions are obtained at photolysis wavelengths corresponding to peaks in the absorption spectrum. We find that the NO stretching vibrations of T_1 evolve adiabatically into NO vibrational excitations [i.e., excitation of v_1 quanta of the T_1 NO stretch yields predominantly NO($v'' = v_1$)]. The NO rotational distributions depend only on the number of T_1 bending quanta, v_3. The shapes of the distributions reflect the number of nodes in the bending wave functions, and similar rotational distributions are obtained following excitation of vibronic levels with equal number of v_3 quanta, but different number of v_1 quanta ($v_1 = 0$–2). We also find that the excited NO($^2\Pi_{3/2}$) state is much more populated than the lower NO($^2\Pi_{1/2}$) state, and the widths of the absorption features increase with increasing number of v_3 quanta, but decrease with increasing v_1 excitation. The results are explained in terms of a model in which the bending and NO stretch motions in the excited state are largely uncoupled. In order to explain the multimodal rotational distributions, we calculate separately the components of the NO rotational excitation that derive from the angular momentum inherent in the bending wave function and the angular anisotropy in the potential-energy surface. We find, using the momentum representation of the harmonic oscillator, that the rotational distributions map the bending wave functions and exhibit minima for $v_3 > 0$. In addition, a unidirectional torque generated by the angular anisotropy in the potential causes shifts in the distributions calculated by the pure Franck–Condon model that are bending level dependent. The observation that the absorption linewidth decreases with increasing NO stretch excitation in the parent T_1 state may be a manifestation of the energy mismatch between the frequency of the NO stretch in NOCl and free NO; the increased mismatch with increasing stretch quantum number results in slower dissociation.

I. INTRODUCTION

An important goal in the study of photodissociation dynamics of small molecules is the understanding of the relationships between the electronic structure of the excited-state and the product-state distributions. The electronic structure determines the shape of the potential-energy surface (PES), and thus the forces and torques that govern the partitioning of the excess energy among the quantum states of the fragments. NOCl promises to be an important prototypical molecule for studying the correspondence between features of the PES and product-state distributions. The Cl and NO fragments have comparable masses and thus kinematic biases do not obscure the dynamics. Also, NOCl has several low-lying dissociative electronic transitions in the visible and near UV which are rather well separated,[1] and were unambiguously assigned recently using a combination of photofragment spectroscopy, vector correlation measurements, and *ab initio* calculations.[2,3] Thus, photodissociation on different electronic surfaces of the same molecule can be studied as a function of photolysis wavelength and compared with theory.[2–9] Previous work on dissociation from several

excited states of NOCl shows striking differences in the NO energy distributions, despite the fact that all the excited states involved in the dissociation result from excitation of a non-bonding electron centered on the Cl atom to a NO π^* orbital. In addition, some of the dissociative states exhibit diffuse structure, and thus the dissociation dynamics from specific vibrational levels in the excited states can be studied. This is the subject of the present work.

In 1983, Solgadi *et al.* published the first *ab initio* configuration-interaction (CI) calculations on NOCl and showed that all its singlet states are repulsive.[8] However, these authors did not include triplet states, nor did they calculate oscillator strengths, and this led to incorrect assignments of the observed transitions in the absorption spectrum.[4,8] More recent CI calculations corrected these deficiencies and also included more complete explorations of the potential-energy surfaces.[2] Based on the new calculations and the experimental results, the bands in the absorption spectra were reassigned, and in particular, the series of diffuse bands between 625 and 525 nm (the E band)[1,2] was assigned to the first singlet–triplet transition arising from excitation of a predominantly $Cl\,p_x + O\,p_x$ electron to the NO π_z^* orbital.[2] The $T_1(1\,{}^3A'') \leftarrow S_0(1\,{}^1A')$ transition dipole moment is typical of a *parallel* transition, since the forbidden transition

---
[a] NSF Predoctoral Fellow.

$(f \sim 10^{-5})$ borrows intensity from the strong $S_5 (4\,^1A') \leftarrow S_0 (1\,^1A')$ parallel band $(f \sim 0.5)$.[2] The E band absorption spectrum exhibits two groups of three peaks (Fig. 1). Each group consists of a progression in ν_3, the NOCl bend ($\nu_3 = 380$ cm^{-1}), and the two groups, which are separated by ~ 1500 cm^{-1}, correspond to the NO stretch in T_1, $v_1 = 0$ and 1.[1,2] Although progressions in both ν_3 and ν_1 are apparent, the measured NO vector properties indicate that the dissociation is still much faster than a rotational period.[2]

In previous publications we reported that dissociation on T_1 leads to a large preference for production of the excited NO($X\,^2\Pi_{3/2}$) spin-orbit state, a noticeable rotational alignment parameter indicating $\mu \perp J$, and a preference for the $\Pi(A'')$ Λ-doublet component.[2,9] A more intriguing result concerns the NO *rotational* distributions which depend sensitively on the number of excited *bending* quanta and are multimodal when $v_3 > 0$.[9] NO *vibrational* excitations, on the other hand, depend only on the number of NO *stretching* quanta in the excited parent.[9]

There exist numerous theoretical models that deal with product excitations following direct photodissociation,[10–16] and the conceptual framework for dealing with these phenomena is well established. However, only few models deal with the consequences of parent vibrational and rotational excitations. Band, Morse, and Freed, in particular, used a Franck–Condon model and developed an analytical description of the photodissociation of linear and bent triatomics.[12,13] They predicted that oscillations in the diatom rotational distributions will occur for bent and/or vibrationally excited triatomic molecules.[12] The exact shapes of the rotational distributions depend on whether the molecule is linear or bent, and on the number of vibrational quanta.[12] These oscillations and their dependence on vibrational quantum number have never been observed experimentally.

In this paper we describe in detail our findings concerning NO V,R distributions following dissociation on T_1. We show that parent NO stretch excitation evolves adiabatically into free NO vibrational excitation, and that the rotational distributions have "nodes" that depend only on the number of nodes in the bending wave function in the excited parent. The model we present to explain these observations is conceptually simple; we propose that the multimodal rotational distributions map the bending wave functions in the excited T_1 state of the dissociating NOCl, but this mapping is modified by a modest torque resulting from the angular anisotropy in the potential. We describe a quantum-mechanical time-dependent harmonic-oscillator model, and show that the main source of NO angular momentum is the NOCl excited-state bending wave functions. This is most easily understood in terms of the momentum representation of the harmonic oscillator,[17] since the wave functions, which are similar in shape to those in coordinate space, have angular momentum nodes for $v_3 > 0$ corresponding to minima in the observed NO rotational distributions. In addition, the torque acquired during the N–Cl bond separation causes a shift in the distributions. With this simple model we are able to simulate the experimental results surprisingly well, and

the model is also in accord with the features of the PES calculated *ab initio*.

II. EXPERIMENTAL

The experimental arrangement is very similar to the one used previously,[2,5] and only details specific to the present experiment are described. Premixed NOCl samples (10/500 Torr in He) were prepared and expanded via a pulsed valve into the fluorescence chamber. The photolysis laser was a Nd:YAG laser-pumped dye-laser system, and the probe laser radiation was obtained from an excimer laser-pumped dye-laser system. The output at 450 nm was frequency doubled with a BBO crystal, and the NO fragments were probed by one-photon laser-induced fluorescence (LIF) via the $A\,^2\Sigma^+ \leftarrow X\,^2\Pi$ transition at ~ 226 nm. The fluorescence was detected with a solar blind photomultiplier tube (PMT) through an interference filter (300 nm, 85 nm bandwidth). The intensity of the probe laser beam (5 mm diam) was maintained at $< 40\,\mu$J in order to avoid saturation, and dissociation of NOCl by the 226 nm radiation in particular. Although the 300 K absorption cross section of NOCl at 226 nm is much larger than at the photolysis wavelengths used in these experiments, dissociation and detection by the probe laser involve sequential absorption of two photons, and this process is largely eliminated when the probe laser intensity is much smaller than the photolysis laser intensity.

The two laser beams were collinear and counterpropagating, but perpendicular both to the PMT and to the pulsed valve. The polarization of the photolysis laser was rotated with a half-wave plate, and the desired polarization component was further selected with a Rochon polarizer. The probe laser was maintained at a vertical polarization. The timing sequence was controlled by a homemade digital delay generator with 20 ns increments, and the delay between the pump and probe lasers was typically $\leqslant 100$ ns. The observed LIF signals were normalized to both laser intensities. Usually, the signals from 30 to 50 laser firings were averaged for each data point.

NOCl (Matheson) was purified by trap-to-trap distillations. Due to the existence of equilibrium between NOCl and NO, it was impossible to completely eliminate NO contamination. However, the expansion-cooled NO contamination gives rise predominantly to $J'' < 5.5$, and the distributions reported here were corrected by carrying out on–off experiments.

III. RESULTS

A. Photofragment yield spectra

Photofragment yield (PHOFRY) spectra are obtained by varying the photolysis laser wavelength while monitoring selected levels of NO($X\,^2\Pi$) 80 ns after dissociation. Several PHOFRY spectra are shown in Fig. 1 and compared with the 300 K absorption spectrum of NOCl. We find that the peaks in the PHOFRY spectra depend strongly on the monitored NO($X\,^2\Pi,v'',J''$) state. In particular, when monitoring low rotational levels in NO($v'' = 0$), only the first group of three peaks is observed, whereas monitoring NO($v'' = 1$)
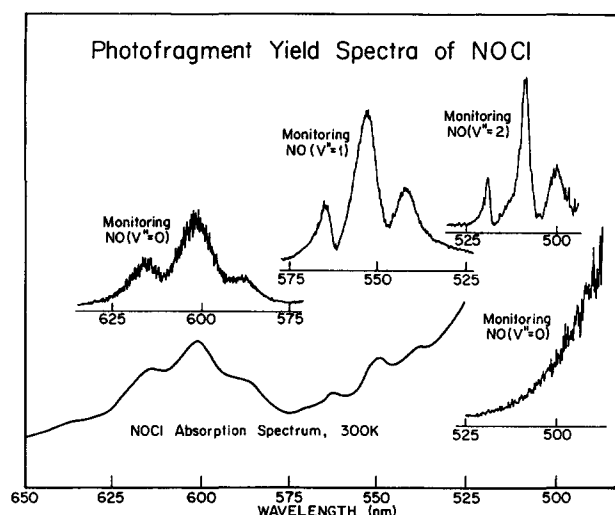
FIG. 1. The absorption and photofragment yield (PHOFRY) spectra of NOCl in the region of the $T_1 \leftarrow S_0$ transition. The absorption spectrum was obtained at 300 K. The other traces show the PHOFRY spectra obtained with jet-cooled samples, and each group of three peaks was obtained by monitoring the P_{22} bandhead ($J'' = 1.5$–4.5) of the NO vibrational level indicated in the figure. The first group consists of, in order of decreasing wavelength, the (000), (001), and (002) bands; the second group consists of the (100), (101), and (102) bands, and the third group of the (200), (201), and (202) bands. The intensities of the different groups are not normalized with respect to one another. The groups are separated by ~ 1500 cm^{-1}, the frequency of the NO stretch, v_1. In the 525–495 nm region, the PHOFRY spectrum obtained by monitoring NO[$v'' = 0$, Q_{22} (33.5)][5] is much more intense than that obtained by monitoring the P_{22} bandhead of NO($v'' = 2$).

FIG. 2. Nascent NO ($X\,^2\Pi_{3/2}$) rotational level distributions obtained following excitation of jet-cooled NOCl at wavelengths corresponding to the peaks in the PHOFRY spectra (Fig. 1). The upper, middle, and lower panels correspond to excitations of $v_3 = 0$, 1, and 2, respectively, in T_1. The panels on the left show the P_{12} and Q_{22} level distributions for NO($v'' = 0$), whereas those on the right show the P_{22} and Q_{22} distributions for NO($v'' = 1$). The results were obtained with $E_{pr}\,\|E_{ph}$, $k_{pr}\,\|k_{ph}$, and vertically polarized E_{pr}. The distributions are not corrected for alignment and Λ-doublet populations differences (see the text and Ref. 2).

yields only the second group of peaks. The reason, of course, is that the PHOFRY spectra correspond to partial absorption spectra, and exhibit only those transitions that correlate with the monitored states of the photofragments. Thus, the state-specific PHOFRY spectra can reveal absorption features that are hidden or overlapped in the total absorption spectrum. This is best illustrated by the PHOFRY spectrum obtained when NO($v'' = 2$) is monitored. The 300 K absorption spectrum at 450–525 nm exhibits a broad structureless band (the D band).[1] The PHOFRY spectrum obtained when monitoring $J'' = 33.5$ of NO($v'' = 0$) reproduces the absorption spectrum very well, and the NO vector properties unambiguously ascribe it to the $S_1(1\,^1A'') \leftarrow S_0(1\,^1A')$ transition.[2,5] In contrast, when monitoring low-J'' levels of NO($v'' = 2$) only weak features, consisting of the three peaks characteristic of the bending progressions of the $T_1 \leftarrow S_0$ transition, appear in the PHOFRY spectrum. Thus, at photolysis wavelengths 490–525 nm, simultaneous absorption to S_1 and T_1 occurs, and the contributions from the two transitions can be revealed only in the state-selective PHOFRY spectra.

The spectra shown in Fig. 1 were all obtained by monitoring the P_{22} bandhead consisting of low NO J'' levels, except for NO($v'' = 0$) obtained following photolysis at 490–525 nm, which was monitored on the Q_{22} (33.5) line.[5] Since the low-J'' lines are the most intense in all the rotational spectra arising from dissociation on T_1 (Fig. 2), the PHOFRY spectra yield the relative intensities of the bands
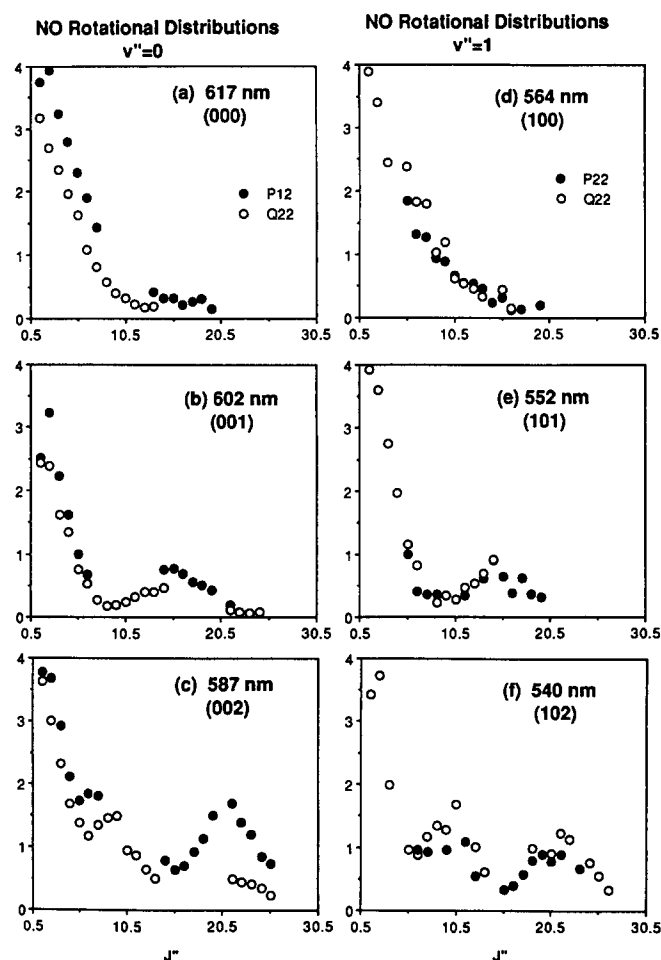
within each bending progression, and peak at $v_3 = 1$. In the NO stretch progression, excitation to $v_1 = 0$ yields the strongest band, in agreement with the changes in geometry between the ground and excited states[2] and the calculated Franck–Condon factors.[18] However, the PHOFRY spectra obtained by monitoring different NO v'' levels are not normalized with respect to one another, and thus the exact relative intensities in a v_1 progression cannot be determined. In addition to the vibrational state specificity exhibited in the PHOFRY spectra, two other features are clearly evident: (i) the linewidth narrows as v_1 increases—from 331 cm^{-1} full width at half maximum (FWHM) for (001) to 262 cm^{-1} for (101) and 116 cm^{-1} for (201); and (ii) within a bending progression, the width increases with increasing bending quanta. For example, in the ($10v_3$) progression, which is fairly well resolved, FWHM equals 157, 262, and 290 cm^{-1} for $v_3 = 0$, 1, and 2, respectively. In addition, we notice that the peaks in the PHOFRY spectra are asymmet-

ric with a slow rise on the red side and an abrupt fall on the blue. This is particularly apparent in the ($10v_3$) and ($20v_3$) progressions which are well resolved.

B. Rotational distributions, spin-orbit, and Λ-doublet populations

The rotational distributions were obtained as described before, and are shown in Fig. 2, uncorrected for rotational alignment.[2] Rotational distributions obtained for NO($v'' = 0$) and NO($v'' = 1$) are shown following excitation in the ($00v_3$) and ($10v_3$) bending progressions, respectively. In each case, the excitation wavelength coincides with a peak in the PHOFRY spectrum. The spectra were obtained by using polarized lasers with $E_{ph} \| E_{pr}$ (the ph and pr subscripts denote the photolysis and probe lasers, respectively). As discussed before, the P_{12} and Q_{22} lines of NO($^2\Pi_{3/2}$) correspond to the $\Pi(A'')$ Λ-doublet component, and their relative intensities should be equal in the absence of alignment.[2] Analyses of rotational spectra obtained at different laser polarizations and geometries [such as those shown in Fig. 2 for NO($v'' = 0$)] yield, in the limit of classical rotation, a rotational alignment characteristic of $\mu \perp J$, in accord with the parallel nature of the NOCl $T_1 \leftarrow S_0$ transition.[2] As expected, Λ-doublet preference is not observed for the low-J'' states; however, excitations in the ($v_1 02$) bands yield $J'' > 20.5$ for which a preference for the $\Pi(A'')$ component is apparent, as discussed before.[2] The transition dipole moment direction, rotational alignment, and Λ-doublet populations were discussed in a previous publication.[2]

The most striking result, however, is the multimodal rotational distributions (Fig. 2) which depend sensitively on the number of *bending* quanta in the upper state, but are independent of the number of NO stretch quanta (v_1).[2,9] We observe that excitation of $v_3 = 0$ yields a cold NO rotational distribution; however, a second peak appears in the distribution when $v_3 = 1$ is excited, while excitation of $v_3 = 2$ leads to two additional peaks. Excitations in the ($20v_3$) bands result in very small signals, so only the spectrum obtained following excitation of the strongest transition (i.e., $v_3 = 1$) was analyzed. The rotational distribution looks similar to those displayed in Figs. 2(b) and 2(e). We note that although only distributions derived from the P_{12}, P_{22}, and Q_{22} branches and obtained with $E_{ph} \| E_{pr}$ are displayed, similar distributions were obtained with $E_{ph} \perp E_{pr}$,[2] and when monitoring other branches. However, since the alignment effects are J dependent,[19] the low-J/high-J ratios are somewhat different when using different laser polarization and detection schemes. We also observe a large propensity (~factor of 5) for the production of the higher spin-orbit state, NO($^2\Pi_{3/2}$), relative to NO($^2\Pi_{1/2}$). Since many rotational lines of NO($^2\Pi_{1/2}$) are overlapped, reliable rotational populations especially for the low-J states could not be derived. Low-J states of NO($v'' = 0$) are affected by contributions from NO contaminations in the beam, and on–off experiments are carried out to correct the intensities. However, when the signal from NOCl is small relative to that originating from the NO contamination, the error in the distributions becomes large.

IV. THEORETICAL MODEL

Several quantum-mechanical theories have been developed to describe photodissociation dynamics,[10-16] and today a full quantum-mechanical calculation can be carried out for simple triatomics provided a complete potential-energy surface is available.[10(d),10(e)] However, in order to gain physical insight, we use a simple model based on a time-dependent harmonic-oscillator Hamiltonian in the bending coordinate to describe the NO rotational distributions following dissociation of NOCl on T_1 ($1\,^3A''$). In this section we describe the model, and discuss the evolution of the molecule on the excited-state surface. The model is based on the experimental finding that the evolution of the T_1 bending and NO stretch excitations are largely uncoupled. Since the NO stretch excitation evolves adiabatically into NO vibration, we assume that at a certain N–Cl separation it becomes uncoupled from the bending and N–Cl stretch modes. Thus, in order to describe the rotational distributions, we only have to deal with the bending mode, which is treated as a harmonic oscillator, and any coupling between modes is incorporated in the time-dependent treatment. Implicit also is the assumption that the v_3 normal mode is a pure NOCl bend.

Since the absorption spectrum exhibits diffuse vibrational structure, we assume that the excited-state bending wave functions are fully developed before dissociation takes place. Therefore, in our model we divide the photodissociation of NOCl on T_1 ($1\,^3A''$) into three steps:

$$\text{NOCl} + h\nu \rightarrow \text{NOCl}^*, \tag{1}$$

$$\text{NOCl}^* \rightarrow \text{NOCl}^{*\prime}, \tag{2}$$

$$\text{NOCl}^{*\prime} \rightarrow \text{Cl} + \text{NO}. \tag{3}$$

The first step is the usual laser excitation and can be well understood by the Franck–Condon approximation. The second step describes the evolution of the initially prepared excited state towards a "critical configuration" before the final fragment separation takes place. The third step is a fast departure of the fragments and, in the absence of couplings between the dissociation coordinate and the other coordinates (i.e., bending and NO stretch), the wave functions in the non-dissociative coordinates are "frozen" at the beginning of this departure and can be expanded in terms of the free fragments' wave functions. This step can be well described by the Franck–Condon model which is applicable to vibrational predissociation as well.[12] Thus, the NO rotational distributions are obtained by projection of the wave function at this critical configuration onto the fragments' wave functions.[10] Although the sharp division into three distinct steps is artificial and, in a full treatment, unnecessary, this description is useful in identifying the sources of angular momenta in the dissociating NOCl. As shown below, the torque generated on T_1 only shifts the rotational distributions relative to those obtained in the Franck–Condon limit. The Franck–Condon picture can still be used for step 3, and the essential condition is that the second and third steps are fairly well separated. This is a reasonable assumption for dissociation on T_1, since the PES is not steeply repulsive at small internuclear separations.[2]

A. Mapping of excited-state wave functions onto fragment rotational distributions

Band, Morse, and Freed,[12,13] and Beswick and Gelbart[11] developed separately a Franck–Condon–type theory to describe the photodissociation of triatomic molecules. We take a similar approach to describe the third step in NOCl photodissociation.

For step 3, if we calculate the NO rotational populations in the Franck–Condon limit, we get that the probability of populating a fragment rotational level j is[10–13]

$$P(j) = |\int \Psi_{\text{bend}}^{*\prime}(\theta) Y_{j0}(\theta,\varphi)\sin\theta d\theta d\varphi|^2 \qquad (4)$$

where $\Psi^{*\prime}$ is the wave function of the parent molecule before the final departure commences (i.e., when the bending potential is just about to disappear), Y_{j0} is the fragment's wave function with $J_{\text{parent}} = 0$, and θ,φ are the usual spherical coordinates in the molecular frame (see Fig. 3), where z is selected to be along R.

Although it is not difficult to calculate the rotational distributions using Eq. (4), we take a different approach to illustrate the physics of the problem. By setting the z axis perpendicular to the molecular plane, we can rewrite the rotational distribution of the diatomic fragment as

$$P(j) = (2j + 1)^{-1}|4\pi^{3/2}\sum_{m'}|Y_{jm'}(\theta' = \pi/2)|^2$$

$$\times \int \Psi_{\text{bend}}^{*\prime}(\varphi')\sin\varphi' \exp(im'\varphi')d\varphi'|^2$$

$$(5)$$

where m' ranges from $-j$ to $+j$ in the summation, φ' is defined in Fig. 3, and $\Psi_{\text{bend}}^{*\prime}(\varphi')$ is the bending wave function of the parent molecule. Different bending wave functions were used to test Eqs. (4) and (5), and the fragment rotational distributions obtained with the two equations were identical.

For high rotational levels of the diatomic fragment (i.e., $j \gg 1$), the $m' = \pm j$ terms dominate in the summation in Eq. (5), and we obtain in the high j limit

$$P(j) \cong 2\pi(|c_j|^2 + |c_{-j}|^2) + \text{interference terms} \qquad (6)$$

where

$$c_{\pm j} = (2\pi)^{-1/2}\int \Psi_{\text{bend}}^{*\prime}(\varphi')\exp(\pm ij\varphi')d\varphi'$$

and we use the fact that

$$8\pi^3|Y_{jj}(\theta' = \pi/2)|^4/(2j + 1) \cong 1.$$

From Eq. (6) we see clearly that $P(j)$ depends on the counterclockwise and clockwise rotational motions inherent in
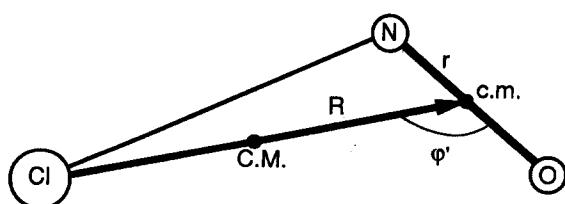

FIG. 3. The coordinate system used in the model calculations. The z axis is perpendicular to the molecular plane.

the bending wave function (i.e., $|c_j|^2$ and $|c_{-j}|^2$, respectively), and the interferences between the two motions, which result in oscillations in the rotational populations.[10–13,20]

Note also that the choice of $\Psi_{\text{bend}}^{*\prime}(\varphi')$ is important. By using the harmonic-oscillator bending wave function centered at φ_0', the equilibrium bending angle, we obtain that the term $|c_j|^2 + |c_{-j}|^2$ in Eq. (6) directly maps the bending wave function of the parent molecule, just prior to the final product separation. However, when using also the wave function centered at $2\pi - \varphi_0'$, interference is obtained which causes extra oscillations in the rotational distributions, superimposed on the smooth mapping.[20] Such oscillations are also obtained when using the analytical formula derived by Morse and Freed,[12(b)] as well as other treatments of the Franck–Condon limit.[11,21] The extra oscillations average out when summing over an initial rotational distribution in the parent, or including final-state interactions,[21] but the nodal pattern originating from the parent vibrational wave function is still preserved.[22] The experimental NO rotational distributions (Fig. 2), do not show these extra oscillations, apparently because of the above-mentioned reasons, and therefore in what follows we neglect the interference effects. This yields essentially the envelope of the oscillations in the product rotational state distribution.[23]

B. The evolution of the parent molecule on the excited surface; a time-dependent harmonic-oscillator description

The Hamiltonian that describes the molecular motion after the laser excitation (i.e., steps 2 and 3) can be expressed in the usual way:[10]

$$H(R,r,\varphi') = \frac{1}{2\mu}P^2 + \frac{1}{2m}p^2 + \left(\frac{1}{2\mu R^2} + \frac{1}{2mr^2}\right)j^2$$

$$+ V(R,r,\varphi'), \qquad (7)$$

where

$$\mu = \frac{m_{\text{Cl}}m_{\text{NO}}}{m_{\text{Cl}} + m_{\text{NO}}}, \quad m = \frac{m_{\text{N}}m_{\text{O}}}{m_{\text{N}} + m_{\text{O}}},$$

$$P = \frac{\hbar}{i}\frac{\partial}{\partial R}, \quad p = \frac{\hbar}{i}\frac{\partial}{\partial r}, \quad j = \frac{\hbar}{i}\frac{\partial}{\partial\varphi'}.$$

For NOCl, the coordinates are indicated in Fig. 3. In the above Hamiltonian, we already assume $\mathbf{J}_{\text{parent}} = 0$, and therefore $\mathbf{j} = -\mathbf{l}$, where l is the orbital angular momentum (neglecting the electronic angular momenta of the fragments). From Eq. (7), it is evident that the bending motion (j, φ') is coupled to the NO stretch (r, p), and the motion in the reaction coordinate (R, P), even when the potential is separable.

To separate the variables, we use an effective time-dependent harmonic-oscillator Hamiltonian for the bending degree of freedom:

$$H(t,\varphi') = B(t)j^2 + \frac{I(t)\omega^2(t)}{2}[\varphi' - \varphi_0'(t)]^2, \qquad (8)$$

where

$$B(t) = \frac{1}{2\mu R^2(t)} + \frac{1}{2mr^2(t)},$$

$$I(t) = 1/[2B(t)], \qquad (9)$$

and ω is the instantaneous bending frequency. $R(t)$ and $r(t)$ in Eq. (9) denote the ensemble average of R and r at any given time. There are several points worth mentioning regarding the Hamiltonian described by Eq. (8). First, $B(\infty)$ is the NO rotational constant, since with increasing R, the first term in Eq. (9) vanishes and the second term approaches the free NO limit. The difference between $B(0)$ and $B(\infty)$ is only about 10%.[24] Second, as the molecule dissociates, one expects the bending force constant to decrease rapidly, and last, $\varphi_0'(t)$ describes how the equilibrium bending angle changes during the dissociation, and we include this term since the calculated PES indicates an angle change during product separation.[2]

To gain physical insight, we first examine the simplest form of Eq. (8), i.e., we set B and φ_0' as constants, and ω as a simple step function. This is equivalent to a case where no torque is exerted during dissociation (i.e., the pure Franck–Condon limit):

$$\omega = \begin{cases} \omega_0, & t \leqslant T \\ 0, & t > T. \end{cases}$$

The simplified Hamiltonian is

$$H = \begin{cases} \dfrac{1}{2I}j^2 + \dfrac{I\omega_0^2}{2}(\varphi' - \varphi_0')^2, & t \leqslant T & (10a) \\[2mm] \dfrac{1}{2I}j^2, & t > T. & (10b) \end{cases}$$

The solution of Eq. (10) is straightforward. When $t \leqslant T$,

$$\Psi_n(\varphi',t) = \exp[-iE_n(t-T)/\hbar]\phi_n(\varphi' - \varphi_0'), \qquad (11)$$

where $\phi_n(x) = a_n H_n(\alpha^{1/2}x)\exp(-\alpha x^2/2)$ is the usual harmonic-oscillator wave function with $\alpha = \omega I/\hbar$. When $t > T$, the unconstrained Hamiltonian (10b) has eigenfunctions of a planar rotor, i.e., $(2\pi)^{-1/2}\exp(im'\varphi')$, $m' = 0, \pm 1,..., \pm j$, and the solution is

$$\Psi_n(\varphi',t) = \sum_{m'} C_{m'}^n (2\pi)^{-1/2}\exp(im'\varphi')$$
$$\times \exp[-E_{m'}(t-T)/\hbar] \qquad (12)$$

with the expansion coefficients given by

$$C_{m'}^n = (2\pi)^{-1/2}\int_0^{2\pi} d\varphi'\,\Psi_n(\varphi',T)\exp(-im'\varphi')$$
$$= (2\pi)^{-1/2}\int_0^{2\pi}\exp(-im'\varphi')\phi_n(\varphi' - \varphi_0')d\varphi'. \qquad (13)$$

If the wave function $\phi_n(\varphi')$ is localized in the angular coordinate (i.e., one can still use a harmonic-oscillator wave function description), the coefficients in Eq. (12) can be evaluated analytically by using the generating function for the Hermite polynomials. However, we choose to present a different approach that highlights the physical significance of the coefficients.

It is well known that one can rewrite the harmonic-oscillator Hamiltonian (10a) in momentum representation.[17] Due to the symmetry of the Hamiltonian, the wave functions in the momentum representation have identical functional forms to those in coordinate space:

$$\phi_n(\hbar j) = a_n H_n(\alpha'^{1/2}\hbar j)\exp(-\alpha'\hbar^2 j^2/2), \qquad (14)$$

where j is the "rotational" quantum number ($\hbar j$ is the angular momentum), and $\alpha' = (I\omega\hbar)^{-1}$. In order to switch from the coordinate representation to the momentum representation one uses a Fourier transformation:

$$\phi_n(\hbar j) = (2\pi)^{-1/2}\int_0^{2\pi}\exp(-ij\varphi')\phi_n(\varphi')d\varphi'. \qquad (15)$$

Comparing Eq. (15) with (13) yields the coefficients

$$C_{m'}^n = \phi_n(\hbar m'). \qquad (16)$$

In Fig. 4 we display, in both representations, the first three bending wave functions of the $T_1(1\,^3A'')$ state of NOCl ($B = 1.96\text{ cm}^{-1}$, $\omega = 380\text{ cm}^{-1}$).

Finally, combining Eqs. (12), (14), and (16), we obtain for this simple Hamiltonian the rotational distributions of the NO fragment when different bending quanta are excited:

$$P_n(j) = 2H_n^2(\alpha'^{1/2}\hbar j)\exp(-\alpha'\hbar^2 j^2). \qquad (17)$$

The NO rotational populations calculated by using Eq. (17) are displayed in Fig. 5. Notice that Eq. (17) describes the Franck–Condon limit of vibrational predissociation, and is similar to Eq. (6), if one neglects the interference terms and uses only the first two terms. [In Eq. (17) we use harmonic-
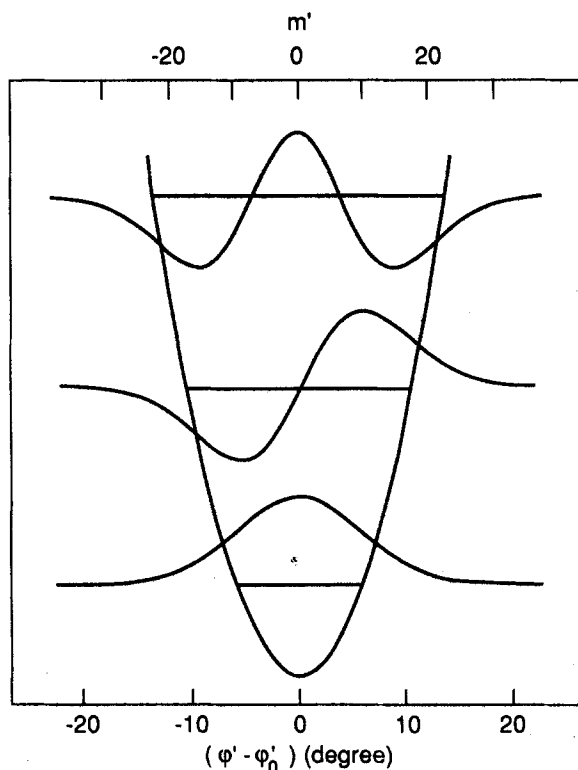

FIG. 4. The harmonic-oscillator bending wave functions used in the model calculations, presented both in coordinate (φ') and momentum (m') space. The following NOCl T_1 bending parameters were used: $B = 1.96\text{ cm}^{-1}$, $\omega = 380\text{ cm}^{-1}$. As expected, the shapes of the wave functions in the coordinate and momentum representations are identical, giving rise to nodes in the angular momentum probability functions which depend sensitively on the number of bending quanta.
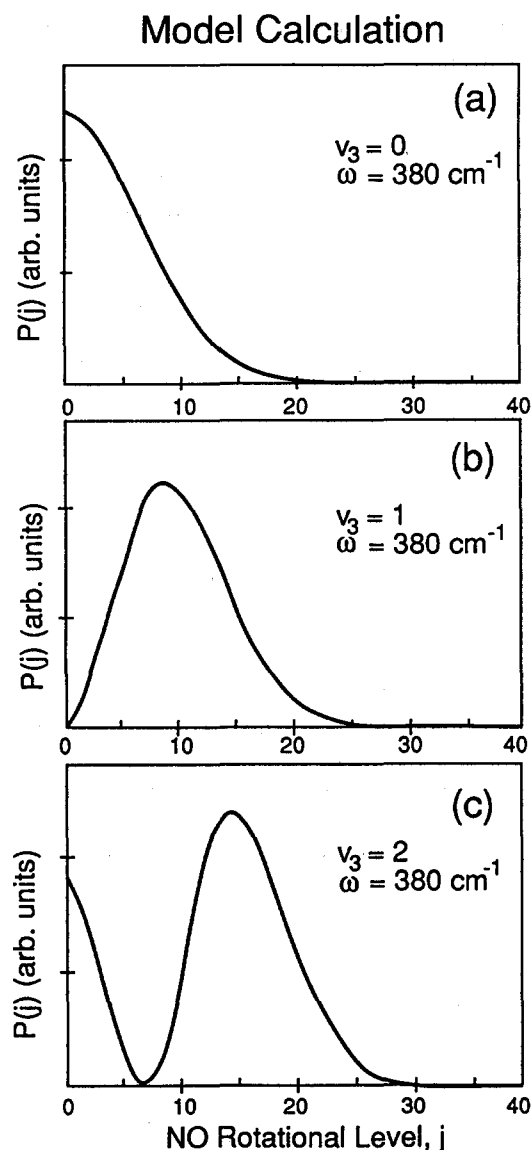
Model Calculation

FIG. 5. NO rotational distributions derived from Franck–Condon projections of NOCl harmonic-oscillator bending wave functions in T_1 onto free NO wave functions [Eq. (17)]. In the calculations, the NO electronic angular momentum and oscillations due to interference effects are neglected (see the text).

oscillator wave functions centered only at φ_0'.] It is clear that even this simple model, which is independent of the details of the PES, gives rise to multimodal rotational distributions.[23] Also, notice that the bending wave function itself contains components of the free-rotor wave function. In other words, the molecular motions that give rise to the harmonic-oscillator bending wave functions include both clockwise and counterclockwise bending motions, resulting in $m' = \pm j$, or clockwise and counterclockwise NO rotations.

We now return to the generalized Hamiltonian [Eq. (8)] and discuss the NO rotational distributions obtained in the dissociation of NOCl. As already mentioned, in NOCl photodissociation $B(t)$ [as well as $I(t)$] changes only by a small amount and therefore this change is neglected. The time-dependent harmonic-oscillator problem can be solved

exactly quantum mechanically in cases where the frequency or the equilibrium angle changes with time. The solutions are given in the literature,[25] and here we discuss only their physical consequences.

If the bending frequency ω decreases slowly with time, the wave functions will adiabatically follow the changing Hamiltonian, and larger α' values need to be used in Eqs. (14) and (17). In this case, we use a weighted average of the bending frequency, $\bar{\omega}$, and we find that the overall rotational distribution shifts towards lower j's in proportion to $(\bar{\omega})^{1/2}$.

The time-dependent equation for zero angle change (i.e., φ_0' as a function of time) can be solved analytically to yield the wave functions[25]:

$$\Psi_n(\varphi',t)$$
$$= \exp\{iJ_1(t)[\varphi' - \varphi_1(t)]\}\phi_n(\varphi' - \varphi_1(t)),\quad (18)$$

where

$$J_1(t) = (I\omega^2/\hbar)\int_0^t \varphi_0'(t')\cos\omega(t-t')dt'\quad (19a)$$

and

$$\varphi_1 = \omega\int_0^t \varphi_0'(t')\sin\omega(t-t')dt'.\quad (19b)$$

The corresponding diatomic rotational distribution is then given by

$$P(j) = F(j - J_1(T)) + F(-j - J_1(T)),\quad (20)$$

where

$$F(x) = H_n^2(\alpha'^{1/2}\hbar x)\exp(-\alpha'\hbar^2 x^2),$$

and $J_1(T)$ is the additional angular momentum caused by the zero angle change. Thus, the angular momentum distribution is shifted in the direction of the torque generated by the change in the equilibrium bending angle during the dissociation.

In the absence of a full PES, we do not know the exact values of $\varphi_0'(t)$ and ω for the dissociating molecule. However, we can use Eq. (20) to simulate the experimentally observed rotational distributions by treating $\varphi_0'(t)$ (i.e., J_1) and ω as adjustable parameters. The results are displayed in Fig. 6, and we note that the best fit is obtained when (i) ω is decreased from the value derived from the absorption and PHOFRY spectra ($380 \, \text{cm}^{-1}$) to $\sim 190 \, \text{cm}^{-1}$; and (ii) J_1 is bending level dependent, i.e., the changes in φ_0' are dependent on the excited-state bending level. The best fits are obtained with $J_1 = 2 \pm 2$, 7 ± 1, and 10 ± 1 for $v_3 = 0$, 1, and 2, respectively.[26] We can get a rough estimate of the changes in φ_0' that correspond to these shifts by looking at Eq. (19a) in the limit of fast angle change. In this case Eq. (19a) reduces to

$$J_1 = (I\omega\varphi_0'/\hbar)\sin\omega T.\quad (21)$$

If we set $\sin\omega T = 1$ (not an unreasonable assumption for $\omega \sim 300 \, \text{cm}^{-1}$, and $T \sim 10^{-13}$ s), and use the appropriate value of I for NOCl, we obtain a J_1 shift of 1.5 angular momentum units per degree change in φ_0'. In the CI calculations, we find that the bending angle changes by 6° when $r_{\text{N–Cl}}$ changes from its equilibrium value of 1.975 to 2.400
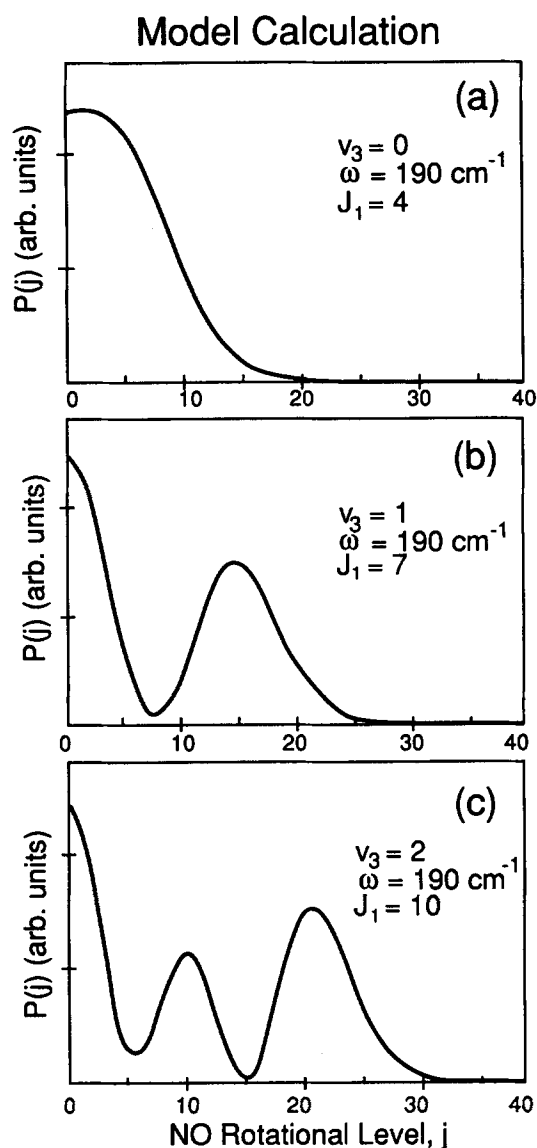
Model Calculation

FIG. 6. NO rotational distributions calculated by using the time-dependent harmonic-oscillator Hamiltonian. The Franck–Condon distributions obtained by using a bending potential with effective frequency ω (which are similar in shape to those shown in Fig. 5) are shifted by torques, J_1, generated during the dissociation on T_1 (see the text for details).

$\text{Å}.^2$ Thus, the angular momentum shifts that are required for best fit are reasonable in view of the angular changes during the dissociation.

Further discussion regarding the physical significance of the assumptions of the model and the results of the calculations is deferred to Sec. V. Here we would like to emphasize only that with this simple model, our goal is not to obtain a quantitative fit to the experimental results, but rather to highlight the sources of angular momenta that evolve into product rotations. Considering the simplicity of the model and the inherent assumptions, the fits we obtain are surprisingly good. Also, as will be shown in Sec. V, the results are in good qualitative agreement with features of the calculated PES.

V. DISCUSSION

A. Summary of the experimental findings

The most important experimental findings obtained in this study are summarized below.

(i) NO stretching vibrations of T_1 evolve adiabatically into free NO vibrational excitations [i.e., excitation of v_1 quanta of v_1 yields predominantly $\text{NO}(v'' = v_1)$].

(ii) The NO rotational distributions show oscillations that depend only on the number of T_1 bending quanta, v_3. The shapes of the distributions reflect the number of nodes in the bending wave functions, and similar rotational distributions are obtained following excitation to vibronic levels with equal number of v_3 quanta, but different number of v_1 quanta ($v_1 = 0$–2).

(iii) The excited $\text{NO}(^2\Pi_{3/2})$ state is much more populated than the lower $\text{NO}(^2\Pi_{1/2})$ state.

(iv) The width of the absorption features in the PHOFRY spectra increases with increasing number of v_3 quanta, but decreases with increasing v_1 excitation.

(v) The peaks in the PHOFRY spectra are asymmetric.

B. Photodissociation model

Although our main goal in this work is to explain the multimodal rotational distributions, the proposed model must rationalize all the experimental observations, and also agree qualitatively with the calculated features of the PES. The full T_1 PES is presently unavailable; however, geometrically optimized least energy paths have been calculated for several points along the N–Cl reaction coordinate,[2] and these are summarized in Table I. The PES along the r_{NCl} coordinate appears to have a shallow minimum, and is rather flat in the region between ~ 2.0 and 2.4 Å. As r_{NCl} increases from 2.1 to 2.4 Å, the ClNO angle decreases from $120°$ to $114°$, and r_{NO} decreases, approaching its equilibrium value for free NO (1.15 Å).[27] The calculated angular potential at $r_{\text{NCl}} = 1.975$ Å and $r_{\text{NO}} = 1.13$ Å is shown in Fig. 7.[2] Notice that as expected for a bending potential of a bent molecule, the potential is asymmetric.

Upon excitation, NOCl accesses the Franck–Condon region of the T_1 PES (i.e., $r_{\text{NCl}} = 1.975$ Å, $r_{\text{NO}} = 1.13$ Å, and $\angle \text{ClNO} = 115°$).[2] Thus, according to the Franck–Condon principle, progressions in v_1 and v_3 are expected, as observed experimentally.[1] The NO stretch and ClNO bend-

TABLE I. Geometrically optimized points on the T_1 ($1\,^3A''$) potential-energy surface of NOCl.[a]

r_{NCl} (Å)	r_{NO} (Å)	$\angle$ClNO (deg)	Energy (eV)[b]
1.975	1.21	120	1.60
2.075	1.17	120	1.18
2.175	1.16	118	1.16
2.400	1.16	114	1.35

[a] From Ref. 2.
[b] Energy relative to S_0 ($1\,^1A'$); $E_{\text{eq}} = -589.154\,168$ a.u. at the calculated minimum energy geometry: $r_{\text{NCl}} = 1.975$ Å; $r_{\text{NO}} = 1.15$ Å, $\angle$ClNO $= 115°$.
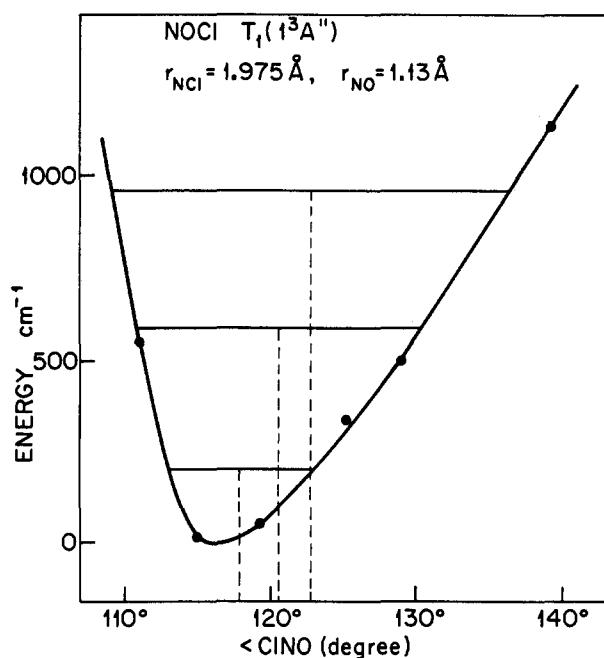
FIG. 7. The NOCl bending potential obtained in the *ab initio* CI calculations (Ref. 2) for $r_{NO} = 1.13$ Å, and $r_{NCl} = 1.975$ Å. The dashed lines show the center angle for each bending level. The center of the wave function does not necessarily coincide with this value, and is probably further shifted to the right due to the asymmetry in the wave function.
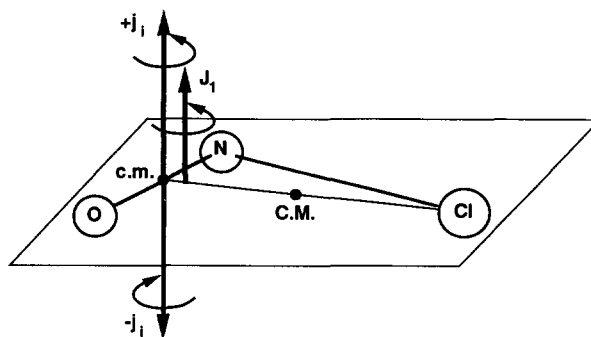

FIG. 8. A pictorial representation of the sources of angular momentum giving rise to the observed NO rotational excitation. The bending wave function is the source of equal clockwise and counterclockwise rotation, $\pm j_i$. In contrast, the angular momentum J_1 generated by the anisotropy in T_1 is unidirectional.

ing wave functions are well developed before dissociation occurs, and the bending wave function remains bound until r_{NCl} reaches at least 2.4 Å (Table I).[2] Since r_{NO} decreases during the initial increase in r_{NCl}, some coupling of the NO stretch coordinate to the r_{NCl} and $\angle$ ClNO coordinates is possible, as discussed below. The decrease in the equilibrium ClNO angle as r_{NCl} increases generates a torque which is a source of NO rotational excitation. Since the bending force constant gradually decreases as r_{NCl} increases, the bending frequency decreases as well. However, at some critical r_{NCl}, we assume that the bending force constant becomes too small to support a vibration and the bending potential suddenly disappears, thereby justifying the use of the Franck–Condon expansion. In the absence of a full PES, we do not know the parameters of this "critical configuration," but estimate it at $r_{NCl} > 2.4$ Å, since at that distance the ClNO angle has already closed and r_{NO} is similar to its free NO value (Table I). Thus, the critical configuration can be described as a "loose transition state." Our model assumes that the dissociation from this point on proceeds along a purely repulsive surface; r_{NO} remains "frozen" and is not coupled any more to the reaction coordinate, and no additional torques are generated in the bending coordinate.

1. NO rotational distributions

In the treatment of rotational excitation, we assume that the bending coordinate can be separated from the other coordinates provided the initial coupling between modes can be included in the time-dependent bending Hamiltonian. We also employ a heuristic division of the dissociation process into three distinct steps in the time domain [Eqs. (1)–(3)].

We then calculate separately the components of the NO rotational excitation deriving from the angular momentum of the harmonic-oscillator bending wave function and the angular anisotropy in the PES. Both sources give rise to in-plane rotation; however, the former results in equal clockwise and counterclockwise rotations, while the latter results in a unidirectional rotation depending on the directionality of the impulse. We have shown analytically how this additional torque shifts the rotational distribution in one direction. The physical interpretation is straightforward; the unidirectional torque is superimposed on the symmetric torque originating from the bending wave function, as shown schematically in Fig. 8. Recall that the angular momentum generated by the bending wave function, j_i, can be either positive or negative, and the distribution of angular momenta in the absence of a unidirectional torque is symmetric about $m' = 0$ (see Fig. 4). Experimentally, we cannot determine the sense of rotation, and $+j_i$ and $-j_i$ deriving from the bending wave function yield the same observed value j [giving rise to the factor of 2 in Eq. (17)]. The situation is different in the presence of a unidirectional torque, J_1. In this case, each observed j in NO corresponds to two different j_i values, $j - J_1$ and $-j - J_1$. In this case, the distribution is symmetric about $m' = J_1$ (see Fig. 4) as described by Eq. (20).

The calculated rotational distributions displayed in Fig. 6 were obtained by treating J_1 and ω as adjustable parameters. The best fit requires $\omega = 190$ cm^{-1} (compared with 380 cm^{-1} for the spectroscopic bending frequency),[1,2] a value which is physically quite reasonable as ω is expected to decrease with the increase in r_{NCl}. As stated above, ω controls the width of the distribution, but not its shape. The shape is determined by the distribution of angular momenta in the bending wave function with its associated nodes, and by J_1. The latter corresponds to changes of up to 6° in the time-dependent equilibrium bending angle, and is in good agreement with the calculated values obtained *ab initio* for the geometry optimized PES.[2] The observation that all the NO distributions peak at low J'' requires that slightly different values of J_1 [or $\varphi'_0(t)$] be used in the simulations for different T_1 bending excitations. This can be rationalized by noting that the bending potential in T_1 is asymmetric (Fig.

7), yielding a different equilibrium angle for each bending level and apparently resulting in slightly different torques.

We thus conclude that the rotational distributions map the excited-state bending wave functions, but this mapping is modified by a modest torque during the dissociation. This is the first time that such mapping has been observed experimentally, and our ability to observe a clear correspondence between the bending wave function and the rotational distribution derives from some unique features of the T_1 PES. It is rather flat in the N–Cl coordinate near the Franck–Condon region, but vibrations are supported in the bending and NO stretch coordinates. It is repulsive at large N–Cl separations, resulting in fast dissociation which can be well described by the Franck–Condon model for vibrational predissociation. The evolutions of the vibrational coordinates are to a large extent uncoupled, and the final-state interactions are relatively weak and do not mask the initial mapping of the bending wave function. Also, the absence of contributions from parent rotations in the jet-cooled samples adds to our ability to identify unambiguously the origins of the NO rotational excitations. The rotational distributions obtained with room-temperature samples exhibit a much less pronounced structure, with the "nodes" almost filled.[22]

The main shortcoming of the present calculations is our ignorance of the exact time-dependent wave functions, necessitating the use of adjustable parameters. We use pure harmonic-oscillator wave functions, and assume that the excitation step [Eq. (1)] is completely uncoupled from the dissociation steps (2 and 3) and can be ignored. In reality, since the dissociation is fast, these steps are probably coupled leading to further deviations from the distributions derived via mapping of the pure harmonic-oscillator wave functions. We also use only $J = 0$, and neglect the extra oscillations due to interferences (see Sec. IV). In addition, the assumption of planarity of the dissociation is not valid for low NO rotational states, and therefore the calculations are less reliable for the low J's. We note that in our experiments, the linewidth of the photodissociation laser is much narrower than the absorption bandwidth. Thus, the excitation does not prepare a well-characterized wave packet in the excited state, and this should also be accounted for in a full treatment. We therefore emphasize that the model described here intends to give a qualitative description of the rotational distributions; it reproduces the width and the nodal structure, but not the exact relative intensities. For example, we observe that the relative intensity of the low-J peak relative to the other peaks, as well as the width of the distributions, are somewhat dependent on the excitation wavelength within each absorption band.[22] It is hoped that more rigorous calculations based on a more complete PES will lead to further refinements in the model.

2. E,V,R,T energy partitioning

The experimental evidence indicates that during dissociation, the NO stretch coordinate in T_1 is largely uncoupled from the other vibrational modes. The optical excitation involves promotion of an electron to the NO π_z^* orbital, and the shape of the PES near the Franck–Condon region apparently promotes the localization of the excitation in this mode

and its adiabatic evolution into free NO vibrational excitation. A somewhat similar situation exists in alkyl nitrites, where in S_1 photodissociation NO stretch excitation in the parent evolves into NO vibrational excitation.[28] However, due to the existence of a well and a barrier in the PES, vibrational predissociation on S_1 leads primarily to population of NO $v'' = v_1 - 1$ following excitation of v_1 NO stretch quanta in RONO.[29] $v'' = v_1$ is also produced, apparently via tunneling through the barrier.[29] In NOCl, since the vibrational frequency in free NO (1860 cm^{-1})[27] is larger than the corresponding v_1 frequency in T_1 (1500 cm^{-1}),[1,2] some V-R,T coupling must take place during the dissociation. Except for this initial coupling, the v_1 excitation remains rather localized during the dissociation. Another consequence of the energy mismatch between the NO frequencies in NOCl and in free NO is the increase in the excited-state lifetime with increasing NO excitation (see below).

By using energy conservation, we can calculate the distribution of the excess energy among the product degrees of freedom. The available energy to be distributed among product rotation and translation is given by

$$E_{\text{avl}} = h\nu - D_0 - E_v(\text{NO}) - E_{\text{el}}(\text{NO}), \qquad (22)$$

where $h\nu$ is the photon energy, D_0 is the dissociation threshold (13 000 cm^{-1}),[30] $E_v(\text{NO})$ is the energy of the NO vibration being monitored, and $E_{\text{el}}(\text{NO})$ is the NO spin-orbit electronic energy. Since NO($^2\Pi_{3/2}$) is predominantly produced in the dissociation, $E_{\text{el}}(\text{NO}) = 123$ cm^{-1}. We assume that Cl is formed in its ground $^2P_{3/2}$ state, but if Cl($^2P_{1/2}$) is produced, 880 cm^{-1} should be subtracted from E_{avl}. The spin-orbit propensities are related to the couplings and uncouplings of angular momenta during the dissociation, and cannot be explained trivially. The average energies obtained for each monitored NO(v'') are summarized in Table II. Excluding vibration, most of the available energy ends up as relative NO and Cl translation, confirming again that the angular anisotropy in the PES, and hence the rotational excitation, is rather small.

TABLE II. Energy partitioning for dissociation on T_1: NOCl$\rightarrow$NO($^2\Pi_{3/2}$,v'') + Cl($^2P_{3/2}$).

NO(v'')	Excitation wavelength (nm)	NOCl v_3	E_{avl}[a] (cm^{-1})	$\langle E_{\text{rot}} \rangle$[b] (cm^{-1})	$\langle E_{\text{tr}} \rangle$[c] (cm^{-1})
0	617	0	3084	90	2994
	602	1	3488	170	3318
	587	2	3912	300	3612
1	562	0	2731	80	2651
	552	1	3117	160	2957
	540	2	3520	340	3180
2	509	1	2799	150	2649

[a] Calculated with Eq. (22), using $E_{v''}(\text{NO}) = 1876$ and 3721 cm^{-1} for $v'' = 1$ and 2, respectively, and $E_{\text{el}}(\text{NO}) = 123$ cm^{-1}.

[b] Since the populations are not corrected for alignment and Λ-doublet effects, the accuracy is only $\pm 20\%$.

[c] The total relative translational energy, $\langle E_{\text{tr}} \rangle$, for each NO($v''$) is given by $E_{\text{avl}} - \langle E_{\text{rot}} \rangle$.

3. Dissociation lifetimes and photofragment yield spectra

As discussed above, measurements of the vector properties (i.e., recoil anisotropies and rotational alignment) indicate that the dissociation lifetimes are much shorter than a rotational period, and thus are probably in the range 10^{-14}–10^{-12} s, as is common in direct dissociation processes. More intriguing is the variation of the linewidths in the PHOFRY spectra with parent vibrational excitation. Within a bending progression, the linewidths increase with increasing v_3 quanta, probably as a result of the anharmonicity in the bending potential (Fig. 7). On the other hand, the absorption linewidths *decrease* by about a factor of 3 in going from $v_1 = 0$ to 2, reflecting an *increase* in the decay lifetimes with the increase in v_1.

One should exercise caution in associating absorption linewidths with dissociation lifetimes. Firstly, the absorption linewidths yield only the dephasing times from the initially excited state, and thus may give only lower limits to the dissociation times. Secondly, in the case of asymmetric line shapes like those shown in Fig. 1, the width may have inhomogenous contributions due to parent rotations, or result from dynamical effects.[31] In our case, since we use expansion-cooled samples, broadening due to a rotational envelope is probably negligible and dynamical effects most likely cause the asymmetry. The lifetimes that correspond to the linewidths of Fig. 1 are 10–30 fs, and in time-dependent wave-packet language, they reflect recurrences in the correlation function near the Franck–Condon region.[16] Similar structured vibrational spectra in fast (<1 ps) dissociating systems has been treated theoretically, using both time-dependent and time-independent formalisms.[16,32] The increasing energy mismatch between the v_1 frequency in NOCl (1500 cm^{-1}) and the NO vibrational frequency (1860 cm^{-1}) requires that energy be transferred from Cl–NO relative translation into NO vibration (we find that the NO rotation does not depend on v_1 excitation); in fact, Table II shows that less energy is available to Cl–NO relative translation as v_1 increases. This would result in slower dissociation from high v_1 levels, and may cause more recurrences in the autocorrelation function, thereby increasing the state's lifetime. Notice also that within a bending progression, both the relative translation and the decay width increase with increasing v_3 (see Table II).

The absorption and PHOFRY spectra indicate that $v_3 = 1$ is the most populated level in a bending progression, and $v_1 = 0$ has the highest population in the NO stretch progression. This agrees well with the relative band intensities inferred from the CI calculations.[18] It is noteworthy that the $(20v_3)$ progression could be seen only in the state-selective PHOFRY spectra, since in the absorption spectrum it is completely overlapped by the much stronger $S_1 \leftarrow S_0$ transition.

VI. CONCLUSIONS

The most intriguing result reported in this paper is the oscillatory nature of the NO rotational distributions whose shapes depend only on the number of bending quanta in the excited T_1 state of NOCl. Although oscillations in fragments

rotational distributions were predicted before,[12] this is the first experimental demonstration of oscillations that can be directly compared with theory. Two unique features of the T_1 PES make these observations possible: (i) The PES is rather flat in the Franck–Condon region, but is repulsive at larger r_{N-Cl} separations, thereby giving rise to diffuse vibrational structure in the absorption spectrum, even though the dissociation is fast. (ii) The modest anisotropy in the PES facilitates the separation of the contributions to the rotational excitation of torques deriving from the bending wave function and from changes in the bending angle during dissociation.

The model we propose reconciles all the experimental observations and is also in accord with the calculated features of the PES. Using a simple, analytical model we identify two sources of rotational excitation: (i) The angular momentum inherent in the bending wave functions, which have nodes in the momentum representation that persist in the rotational distributions. The torques generated by the bending motion give rise to equal clockwise and counterclockwise NO rotations, and the rotational distributions can be calculated by using the Franck–Condon model of photodissociation. (ii) A unidirectional torque resulting from the angular anisotropy in the PES causes a shift in the rotational distributions compared to the pure Franck–Condon picture. The magnitude of the torque can be estimated from best fits to the experimental results, and is in agreement with that derived from the calculated bending angle change during dissociation. It is, however, bending level dependent probably as a result of the asymmetry in the bending potential. Experimentally, we observe that the NO rotational distributions depend only on the number of bending quanta in the T_1 state, and not on NO stretch excitation which evolves adiabatically into NO vibration. The observation that the dissociation time increases with increasing NO stretch excitation in the parent T_1 state is a manifestation of the energy mismatch between the frequency of the NO stretch in NOCl and free NO; the increased mismatch with increasing stretch quantum number results in slower dissociation.

ACKNOWLEDGMENTS

[1] C. F. Goodeve and S. Katz, Proc. R. Soc. London Ser. A **172**, 432 (1939).
[2] Y. Y. Bai, A. Ogai, C. X. W. Qian, L. Iwata, G. A. Segal, and H. Reisler, J. Chem. Phys. **90**, 3903 (1989).
[3] According to the spectral assignments of Ref. 2, the D and C absorption bands (Ref. 1) arise from excitation to S_1 ($1\,^1A\,''$), while excitations to S_3 ($2\,^1A\,'$), S_5 ($4\,^1A\,'$), and T_1 ($1\,^3A\,''$) give rise to the B, A, and E absorption bands, respectively.
[4] A. E. Bruno, U. Brühlmann, and J. R. Huber, Chem. Phys. **122**, 155

(1988); A. Ticktin, A. E. Bruno, U. Brühlmann, and J. R. Huber, *ibid.* **125**, 403 (1988).

[5] A. Ogai, C. X. W. Qian, L. Iwata, and H. Reisler, Chem. Phys. Lett. **146**, 367 (1988).

[6] G. E. Busch and K. R. Wilson, J. Chem. Phys. **56**, 3655 (1972).

[7] (a) M. D. Moser, E. Weitz, and G. C. Schatz, J. Chem. Phys. **78**, 757 (1983); (b) Chem. Phys. Lett. **82**, 285 (1981).

[8] D. Solgadi, F. Lahmani, C. Lardeux, and J. P. Flament, Chem. Phys. **79**, 225 (1983).

[9] C. X. W. Qian, A. Ogai, L. Iwata, and H. Reisler, J. Chem. Phys. **89**, 6547 (1988).

[10] For recent reviews, see, for example, (a) M. Shapiro and R. Bersohn, Annu. Rev. Phys. Chem. **33**, 119 (1982); (b) G. G. Balint-Kurti and M. Shapiro, in *Photodissociation and Photoionization*, edited by K. P. Lawley (Wiley, New York, 1985), p. 403; (c) K. F. Freed and Y. B. Band, in *Excited States*, edited by E. Lim (Academic, New York, 1978) Vol. 3; (d) R. Bersohn, in *Molecular Photodissociation Dynamics* (Royal Society of Chemistry, London, 1987), p. 1; (e) R. Schinke, Annu. Rev. Phys. Chem. **39**, 39 (1988).

[11] J. A. Beswick and W. M. Gelbart, J. Phys. Chem. **84**, 3148 (1980).

[12] (a) M. D. Morse and K. F. Freed, J. Chem. Phys. **74**, 4395 (1981); (b) **78**, 6045 (1983); (c) Chem. Phys. Lett. **74**, 49 (1980).

[13] (a) M. D. Morse, K. F. Freed, and Y. B. Band, J. Chem. Phys. **70**, 3604 (1979); (b) **70**, 3620 (1979).

[14] (a) R. W. Heather and J. C. Light, J. Chem. Phys. **78**, 5513 (1983); (b) **79**, 147 (1983).

[15] H. Grinberg, K. F. Freed, and C. J. Williams, J. Chem. Phys. **86**, 5456 (1987).

[16] (a) E. J. Heller, J. Chem. Phys. **68**, 2066 (1978); (b) **68**, 3891 (1978); (c) Acct. Chem. Res. **14**, 368 (1981).

[17] E. Merzbacher, *Quantum Mechanics* (Wiley, New York, 1961); L. D. Landau and E. M. Lifshitz, *Quantum Mechanics* (Pergamon, Oxford, 1977).

[18] Y. Y. Bai and G. A. Segal (unpublished).

[19] R. N. Zare, *Angular Momentum* (Wiley, New York, 1988).

[20] We thank Moshe Shapiro and Reinhard Schinke for pointing out to us the sources of the interferences.

[21] P. Andresen and R. Schinke, in *Molecular Photodissociation Dynamics*, (Royal Society of Chemistry, London, 1987), p. 61, and references cited therein; R. Schinke, V. Engel, and V. Staemmler, J. Chem. Phys. **83**, 4522 (1985).

[22] A. Ogai, C. X. W. Qian, and H. Reisler (unpublished).

[23] The NO rotational distributions obtained via Eq. (6) when neglecting interference effects are similar to the envelopes of the distributions obtained via Eq. (4) [Refs. 11 and 12(b) for $J = 0$], or Eq. (6).

[24] $B_{NO} = 1.70 \text{ cm}^{-1}$; $B_{NOCl} = 1.96 \text{ cm}^{-1}$.

[25] See, for example, *Problems in Quantum Mechanics*, edited by D. terHaar (Pion, 1975), Chap. 3.

[26] Similar results are obtained when including the interference effects, but the nodal structure is then less apparent, and the agreement with the experimental results is less obvious.

[27] G. Herzberg, *Spectra of Diatomic Molecules* (Van Nostrand, Princeton, 1950).

[28] H. Reisler, M. Noble, and C. Wittig, in *Molecular Photodissociation Dynamics* (Royal Society of Chemistry, London, 1987), p. 137, and references cited therein; O. Benoist d'Azy, F. Lahmani, C. Lardeux, and D. Solgadi, Chem. Phys. **94**, 247 (1985).

[29] M. Nonella and J. R. Huber, Chem. Phys. Lett. **131**, 376 (1986); S. Hennig, V. Engel, R. Schinke, M. Nonella, and J. R. Huber, J. Chem. Phys. **87**, 3522 (1987); M. Nonella, J. R. Huber, A. Untch, and R. Schinke, *ibid.* (in press).

[30] *JANAF Thermochemical Tables*, 2nd ed., edited by D. R. Stull and H. Prophet, Natl. Stand. Ref. Data Ser. Natl. Bur. Stand (U.S. GPO, Washington, D. C., 1967).

[31] S. Henning, A. Untch, R. Schinke, M. Nonella, and J. R. Huber, Chem. Phys. **129**, 93 (1989).

[32] R. Pack, J. Chem. Phys. **65**, 4765 (1976).